Coherent control of nanoscale localization of ultrafast optical excitation in nanosystems

Mark I. Stockman,[1,*] David J. Bergman,[2,†] and Takayoshi Kobayashi[3,‡]
[1]*Department of Physics and Astronomy, Georgia State University, Atlanta, Georgia 30303, USA*
[2]*School of Physics and Astronomy, Raymond and Beverly Sackler Faculty of Exact Sciences, Tel Aviv University, Tel Aviv 69978, Israel*
[3]*Department of Physics, University of Tokyo, Hongo 7-3-1 Bunkyo-Ku, Tokyo 113-033, Japan*
(Received 25 September 2003; published 13 February 2004)

We predict and theoretically investigate the unique possibility to control distribution of ultrafast local optical fields in nanosystems in space with nanometer resolution and in time on the femtosecond scale. While the spatial degrees of freedom of the optical radiation do not allow focusing of the light on nanoscale, the phase of the excitation light constitute a functional degree of freedom that permits one to coherently control the distribution of the energy of local fields, concentrating it at a desired location at certain times. We study both a specially designed V-shaped nanostructure and a random planar nanocomposite. Several types of exciting pulses are investigated, which has allowed us to distinguish effects of phase modulation and spectral composition of the excitation pulse. Possible applications of this effect include energy supply and control of ultrafast optical computations in nanostructures, local optical probing of nanosystems, including nanosensors of chemical and biological agents, and nanomodification of surfaces (nanolithography).

DOI: 10.1103/PhysRevB.69.054202 PACS number(s): 78.47.+p, 42.50.Md, 78.67.−n, 78.20.Bh

I. INTRODUCTION

This paper is devoted to theoretical investigation of the processes of energy localization in space on a nanometer scale and in time on a femtosecond scale in nanosystems and coherent control of such processes. The idea of the coherent control is based on excitation of a coherent packet of quantum states or classical waves that interfere in the processes of the evolution of the system. In the processes of excitation, the different constituent waves of that coherent packet are generated with individual, controllable phases. These phases represent the degrees of freedom that allow one to exert control over that system's evolution.[1–3] In the case of short-pulse excitation, for the coherent control to be efficient, the excitation time should be much shorter than the dephasing times in the system. For metal-dielectric nanosystem this requires ultrashort, femtosecond excitation laser pulses.

From both the fundamental and applied points of view, there are compelling reasons to consider phenomena that are simultaneously ultrafast and localized on nanoscale. Interactions between different parts of a nanosystem are very strong due to small, nanoscale distances separating them. At optical frequencies, a universal part of such interactions at the intermediate to large scales is the dipole-dipole interaction, while at the minimum scale all multipoles should be taken into account. Such interactions on the nanoscale lead to femtosecond times of energy and polarization transfer and relaxation within the nanosystem. On the other hand, ultrashort external excitation allows one to preserve excitation energy and temporal coherence of the nanosystem, which opens up possibilities of coherent control. Additionally, nanosize eliminates effects of electromagnetic retardation and thus facilitates coherent ultrafast kinetics. The phenomena that are nanoscale and ultrafast have recently attracted significant attention, see, e.g., Refs. 4–20.

The applications of ultrafast-nanoscale processes include, but not limited to, time resolved nanoscale probing and detection, in particular nano-Raman spectroscopies, nanomodification of nanosystems where ultrafast excitation and relaxation of the processes helps preserve nanoscale spatial resolution, and computing with the nanoscale devices where femtosecond cycle time is an ultimate goal for ultrafast computations. The coherent control over the spatiotemporal localization of the excitation energy may be useful for a range of nanophotomodification and probing approaches, including those suggested, quite early, in Ref. 21. Among the possible applications is optical drilling of nanoholes in different substrates, nonlinear and Raman nanoprobing of single molecules that was carried out recently using the surface-enhanced Raman scattering (SERS),[22,23] and Raman microscopy and spectroscopy of separate chemical groups of macromolecules, a technique demonstrated recently.[24] For the biological and defense applications the coherent control in Raman spectroscopy of single biological objects such as viruses, spores, and cells and their fragments is promising. An interesting perspective application may be the coherent control of the optical excitation of the proposed spaser, a quantum generator of high-intensity coherent local fields.[19]

The general challenge in optically controlling the spatial distribution of optical excitation of a nanosystem is that optical radiation lacks its spatial degrees of freedom on the nanoscale: within a nano-object, any electromagnetic wave appears as a *spatially uniform* electric field oscillating in time at optical frequencies. The only remaining functional degrees of freedom are the temporal ones: the frequency spectrum and phase of the exciting electric field. Posing an additional problem, the universal, long-range dipole interaction induces ultrafast transfer of excitation in nanostructures,[16] which causes redistribution of the excitation energy across a nanosystem and may lead to delocalization. For instance, consider a local excitation of the system using a near-field scanning optical microscope (NSOM) or a nanoaperture. In this case, the source of the excitation is indeed well localized, but this initially localized excitation will spread over the entire nanosystem on the atto- to femtosecond scale due to the dipolar interaction between differ-

ent parts of the nanosystem.[16,17] Note that additionally, NSOM's or nanoaperture's spectral bandwidth may be insufficient to conduct the *ultrafast* localized excitation.

To solve this problem, we have recently proposed to modulate the phase of an exciting femtosecond pulse as a functional degree of freedom to coherently control spatial distribution of the excitation energy.[18] This possibility exists due to the fact that polar excitations, which are conventionally called surface plasmons (SP's) in inhomogeneous nanosystems, tend to be localized with their oscillation frequency (and, consequently, phase) correlated with the position inside the system.[25–28] The pulse phase modulation will cause the exciting field to take energy away from SP's localized in those parts of the system where the oscillations are out of phase with the driving pulse and move it, with time, to the SP excitations in other parts where such oscillations occur in phase with the driving pulse. Alternatively, one may think that the ''instantaneous frequency'' of the exciting pulse is changing, causing rapid adiabatic passage through the resonance with a localized mode. As a result, this mode will initially be excited and later, as the pulse progresses, deexcited and its excitation energy moved to the next group of modes and further in the frequency domain in the same manner. Because the frequency and localization in space for the eigenmodes of a nanosystem are correlated, it will lead to the flow of the excitation energy in space allowing for the directed localization of the entire excitation energy at a given site of the nanosystem.

Coherent control has been successfully used to spectrally concentrate the energy of an ultrashort nonlinearly generated pulse in a given high harmonic.[29] Predictions have been made of the coherent control over spatial movement of particles and polarization using continuous-wave fields (see, e.g., Refs. 30,31, and references cited therein). Following these predictions, charge-free spin currents of electrons in semiconductors have been observed.[32,33] The possibility has been shown to concentrate the energy of acoustic waves at a given time and site inside a region when these waves are generated by a laser excitation of the surface of that region.[34] Spatiotemporal behavior of phonon-polariton waves in crystals has been achieved by means of coherent control.[35] Sideband THz generation in quantum well/optical microcavity systems, coherently controlled, has been demonstrated theoretically.[36] Later, coherent control has been used to control the vibrational excitations of molecules under nonresonant conditions.[37] A phase-modulated ultrashort pulse serves as a specific ''reagent'' to selectively excite desired chemical transformations.[2,3] Our approach is based on the same general idea of interference between different components of the resonant exciting radiation, governed by the phase modulation. However, it is different, because it requires ultrashort pulses to preserve the coherence in time in contrast to Refs. 30 and 31, but it is a linear effect unlike Refs. 29,31–33, and it results in the concentration of energy in the space on the nanoscale and not on the microscale to macroscale as in Refs. 34 and 35. We differ from Ref. 3 by our relying on the spatial-frequency correlations for chaotic eigenmodes of the complex composite nanosystems.

With respect to the original paper,[18] most of this paper's material is significantly new. In Sec. II, we give the derivation of the spectral expansion for the retarded Green's function, which is the basis of both the analytic theory and numerical computations. In Sec. III, we present numerical procedures that were not described in Ref. 18 in any detail. Section IV presents the original results for transform-limited (compressed) pulses and compares them with the kinetics for the chirped pulses. Such a comparison has allowed us to distinguish effects of the excitation pulse spectrum, its phase modulation, and temporal shape. In particular, it is shown that the ultrashort (single-period) exciting pulse is not the optimum one for achieving the spatial localization of energy on the nanoscale. New results are presented for the averaged intensity of the local fields and the rates of two-photon excitation that is the first optically nonlinear process whose nanoscale spatial distribution is coherently controllable.

II. THEORY: EIGENMODES, GREEN'S FUNCTIONS, AND ULTRAFAST DYNAMICS

We consider a nanosystem whose maximum size L is much less than light wavelength λ. We also assume that the skin-layer thickness greatly exceeds the minimum scale of the system. Under these conditions, we can neglect the spatial dependence of the excitation field that, within the system, can be approximated as a uniform electric field, $\mathbf{E}_0(\mathbf{r},t) = \mathbf{E}_0(t)$, oscillating in time t at optical frequencies. Wave's magnetic component is unimportant under the conditions of this paper and will not be considered. This constitutes the well-known quasistatic approximation, whose name does not imply that the processes under consideration are considered as slow. To the opposite, as we have discussed above in Sec. I, under such conditions, photoprocesses may potentially be extremely fast.

We describe the material system as a continuous inhomogeneous medium with a local dielectric function $\varepsilon(\mathbf{r},\omega)$ that at any point $\mathbf{r}$ of the system depends on excitation frequency ω. The corresponding quasistatic, continuity equation is

$$\boldsymbol{\nabla}\cdot[\varepsilon(\mathbf{r},\omega)\boldsymbol{\nabla}\varphi(\mathbf{r},\omega)]=0, \tag{1}$$

where the frequency argument of field potential denotes the Fourier domain. We consider a system to be confined in a rectangular prizm $0\leqslant x\leqslant L_x$, $0\leqslant y\leqslant L_y$, $0\leqslant z\leqslant L_z$. We impose the conventional mixed Dirichlet-Neumann boundary conditions,

$$\begin{aligned}
&\varphi(\mathbf{r},\omega)=\varphi_0(\mathbf{r},\omega)\big|_{z=0,L_z},\\
&\frac{\partial\varphi(\mathbf{r},\omega)}{\partial x}=\frac{\partial\varphi_0(\mathbf{r},\omega)}{\partial x}\bigg|_{x=0,L_x},\\
&\frac{\partial\varphi(\mathbf{r},\omega)}{\partial y}=\frac{\partial\varphi_0(\mathbf{r},\omega)}{\partial y}\bigg|_{y=0,L_y},
\end{aligned} \tag{2}$$

where $\varphi_0(\mathbf{r},\omega)$ is the potential of the external excitation field, which is also the volume-average electric-field potential. In specific computations, this field is assumed to be uniform and z polarized, so

$$\varphi_0(\mathbf{r},\omega) = -E_0(\omega)z. \tag{3}$$

Note that the analytical results presented below in this chapter remain valid if the Dirichlet boundary conditions were imposed on all six faces of the volume, and also for the periodic boundary conditions. The specific choice of the mixed boundary conditions is due to the fact that we use this method not only for analytical derivations but also in numerical computations where the mixed boundary conditions, as experience shows, are beneficial for efficiency.[46]

In what follows, we will assume the nanosystem consisting of two components with uniform compositions. One of these components, which will be called the host, is assumed to possess dielectric constant ε_h. The second is the inclusion, normally metallic or semiconductor, component with the dielectric function $\varepsilon_i(\omega)$. We will use the spectral theory of Bergman-Milton[38,39] in the differential-equation form of Ref. 28. The dielectric function of the system can be cast into form $\varepsilon(\mathbf{r},\omega) = \Theta(\mathbf{r})\varepsilon_i(\omega) + [1-\Theta(\mathbf{r})]\varepsilon_h$, where $\Theta(\mathbf{r})$ is the characteristic function of the inclusion equal 1 inside that component and equal 0 otherwise. We will use spectral parameter

$$s(\omega) \equiv \frac{\varepsilon_h}{\varepsilon_h - \varepsilon_i(\omega)}. \tag{4}$$

We present the solution total field $\varphi(\mathbf{r},t)$ as the sum of external field $\varphi_0(\mathbf{r},t)$ and the induced field that we denote as $\psi(\mathbf{r},t)$. Setting $\varphi(\mathbf{r},t) = \varphi_0(\mathbf{r},t) + \psi(\mathbf{r},t)$ and taking into account that the function $\varphi_0(\mathbf{r},t)$ is harmonic, we obtain from Eq. (1) an equation for induced field $\psi(\mathbf{r},t)$ as

$$\begin{aligned}\boldsymbol{\nabla}\cdot[\Theta(\mathbf{r})\boldsymbol{\nabla}\psi(\mathbf{r},\omega)] - s(\omega)\nabla^2\psi(\mathbf{r},\omega) \\ = -\boldsymbol{\nabla}\cdot[\Theta(\mathbf{r})\boldsymbol{\nabla}\varphi_0(\mathbf{r},\omega)].\end{aligned} \tag{5}$$

This induced field satisfies the homogeneous Dirichlet-Neumann boundary conditions,

$$\psi(\mathbf{r},\omega)\big|_{z=0,L_z} = 0,$$

$$\left.\frac{\partial\psi(\mathbf{r},\omega)}{\partial x}\right|_{x=0,L_x} = \left.\frac{\partial\psi(\mathbf{r},\omega)}{\partial y}\right|_{y=0,L_y} = 0, \tag{6}$$

Following Ref. 28, we introduce a generalized eigenproblem defined by the following homogeneous equation in partial derivatives [cf. Eq. (5)]

$$\boldsymbol{\nabla}\cdot[\Theta(\mathbf{r})\boldsymbol{\nabla}\varphi_n(\mathbf{r})] = s_n\nabla^2\varphi_n(\mathbf{r}), \tag{7}$$

where $\varphi_n(\mathbf{r})$ are the eigenfunctions that satisfy the same homogeneous boundary conditions of Eq. (6) as the induced field $\psi(\mathbf{r})$, and s_n are the corresponding eigenvalues. Importantly, this eigenproblem depends only on the geometry of the system, but not on its material composition.

The physical eigenmodes defined by this equation are SP's whose complex frequencies $\omega_n + i\gamma_n$ are found from the complex equation

$$s(\omega_n + i\gamma_n) = s_n. \tag{8}$$

For weak relaxation, $\gamma_n \ll \omega_n$, one finds that the real part of the SP frequency ω_n satisfies the equation

$$\mathrm{Re}[s(\omega_n)] = s_n, \tag{9}$$

and that the SP spectral width γ_n is expressed as

$$\gamma_n = \frac{\mathrm{Im}[s(\omega_n)]}{s_n'}, \qquad s_n' \equiv \left.\frac{d\,\mathrm{Re}[s(\omega)]}{d\omega}\right|_{\omega=\omega_n}. \tag{10}$$

Note that these classical SP's have been quantized in Ref. 19 in connection with the prediction of spaser, a nanoscale counterpart of laser.

All functions satisfying boundary conditions (6) and possessing second-order derivatives constitute a linear space that we denote $\mathbb{R}$. Consider two functions, $\psi_1(\mathbf{r}) \in \mathbb{R}$ and $\psi_2(\mathbf{r}) \in \mathbb{R}$. For such functions, we can define a scalar product as the following operation:

$$(\psi_1|\psi_2) = -\int_V \psi_2^*(\mathbf{r})\nabla^2\psi_1(\mathbf{r})d^3r, \tag{11}$$

where $V = L_xL_yL_z$ is the volume of the system. This construction possesses all the necessary and sufficient properties of a scalar product: it is a binary, Hermitian self-adjoined, and positive-defined operation. Note that if at least one of the functions $\psi_1(\mathbf{r}) \notin \mathbb{R}$ or $\psi_2(\mathbf{r}) \notin \mathbb{R}$, but still both of them are twice differentiable, then bilinear form Eq. (11) obviously exists, but it does not necessarily satisfy the scalar product postulates of being positive defined and Hermitian.

From Eqs. (6), (7), and (11), it follows that these eigenfunctions are orthogonal with respect to the scalar product of Eq. (11) and can be normalized,

$$(\varphi_n|\varphi_m) = \delta_{nm}, \tag{12}$$

all eigenvalues s_n are real, and all eigenfunctions $\varphi_n(\mathbf{r})$ can be chosen to be real. Straightforwardly, it can also be shown that all eigenvalues are limited, $1 \geqslant s_n \geqslant 0$, which is expected because the differential equation formulation[28] of the eigenproblem employed in this paper is equivalent to the integral equation formulation where this property is known.[38,39]

To be able to express the solution of the excitation problem [Eqs. (5) and (6)] in terms of the eigenvalues and eigenfunctions, we have to impose a homogeneous Dirichlet boundary condition for the characteristic function Θ,

$$\Theta(\mathbf{r},\omega)\big|_{x=0,L_x} = \Theta(\mathbf{r},\omega)\big|_{y=0,L_y} = \Theta(\mathbf{r},\omega)\big|_{z=0,L_z} = 0. \tag{13}$$

Though necessary in our approach, this additional boundary condition is not restrictive for a finite system, since one can always position the boundary planes outside the volume occupied by the system, in which case Eq. (13) is satisfied automatically. From Eqs. (5)–(7) and (11)–(13), we obtain the spectral expansion for the total field (cf. Ref. 38),

$$\varphi(\mathbf{r},\omega) = \varphi_0(\mathbf{r},\omega) + \sum_n \frac{s_n\ \varphi_n(\mathbf{r})}{s(\omega) - s_n}(\varphi_0|\varphi_n)^*. \tag{14}$$

Note that $\varphi_0(\mathbf{r},\omega) \notin \mathbb{R}$, therefore $(\varphi_0|\varphi_n) \neq (\varphi_n|\varphi_0)$, where in fact $(\varphi_n|\varphi_0)=0$ since φ_0 is harmonic.

We introduce a retarded Green's function as a spectral expansion in the coordinate-frequency domain:

$$G^r(\mathbf{r},\mathbf{r}';\omega)=\sum_n \frac{s_n}{s(\omega)-s_i}\varphi_n(\mathbf{r})\varphi_n(\mathbf{r}')^*. \qquad (15)$$

Note that SP's correspond to the poles of $G^r(\mathbf{r},\mathbf{r}';\omega)$ [cf. Eq. (8)] in accord with the general properties. From Eq. (14), it follows that the electric field potential in the real space and time domain can be expressed as a contraction,

$$\varphi(\mathbf{r},t)=\varphi_0(\mathbf{r},t)-\int_V d^3r' \int_{-\infty}^{\infty} dt' \varphi_0(\mathbf{r}',t')\nabla'^2 \times G^r(\mathbf{r},\mathbf{r}';t-t'). \qquad (16)$$

Spectral expansion results of Eq. (15) and the total electric field potential as the Green function contraction of Eq. (16) represent the basis for both the analytical theory and method of numerical computations that we employ.

III. NUMERICAL PROCEDURES

A few remarks regarding the present approach are due. The spectral expansion employed in the present paper offers the known principal advantage, namely, separation of geometric and material properties. Specifically, the eigenproblem of Eqs. (6) and (7) depends only on geometry of the nanosystem *via* the characteristic function $\Theta(\mathbf{r})$, but not on its material composition. Numerically, this eigenproblem is solved once for a given geometry, which is the most complicated and time-consuming part of the procedure. After the eigenproblem is solved, for any material composition of the system, Green's function in the real space and frequency domain $G^r(\mathbf{r},\mathbf{r}';\omega)$ is computed from Eq. (15) without solving any additional equations. Green's function in real space-time $G^r(\mathbf{r},\mathbf{r}';t-t')$ is then found by fast Fourier transform (FFT) and stored. Then, the fields for any specific material composition for any point in space and time can be computed by numerical integration from Eq. (16).

This approach is quite efficient with respect to the CPU time, though it requires a significant (multigigabyte) memory for the required size of the system (the required memory scales as sixth power of system's geometric size). However, it is chosen by us not because of the efficiency considerations, but because of its exceptionally high numerical stability, which is due to the following. Owing to its structure, the spectral expansion Eq. (15) automatically possesses the exact analytical properties of a retarded Green's function: it has only simple poles, and, provided that the constituent dielectric functions satisfy the Kramers-Kroning dispersion relations, it is causal, i.e., all those poles are in the lower half plane. We emphasize that that these analytical properties are exactly satisfied by the form of the spectral expansion of the Green's function, no matter how accurately the eigenproblem is approximated, as long as the eigenfunctions found are orthonormal. Importantly, this prevents violation of the causality, which is a nontrivial property for any Fourier-based method.

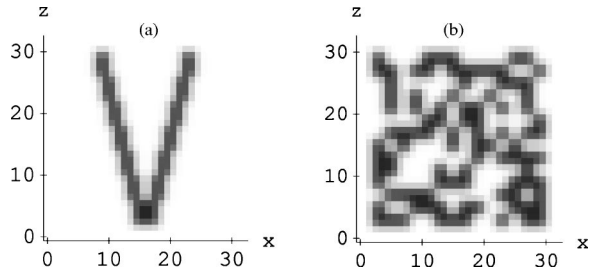

FIG. 1. Nanosized metallic inclusions in the central xz plane: (a) Engineered V shape and (b) random planar composite (RPC). Distances are expressed as grid steps, with one step corresponding to a distance of 3–5 nm (see text).

We have discretized Eqs. (6) and (7) on a three-dimensional rectangular grid of size $n_x \times n_y \times n_z$ whose dimensions (in the grid steps) are: $n_x=n_z=32$; $n_y=8,16$, and 32. We use a third-order discretization scheme. The obtained results show no qualitative dependence on n_y within the range indicated. This was expected from the investigation of the sensitivity of the eigenmodes and eigenvalues to the grid size studied in Ref. 28. After the discretization, the obtained linear generalized eigenproblem is solved by using a highly efficient, multithread realization of the LAPACK linear algebra package[40] for Itanium 2 processors.[41]

The systems studied are planar metal nanostructures positioned in the central x,z plane whose thickness (in the y direction) is two grid steps. The nanostructures of two geometries have been employed displayed in Fig. 1: a specially engineered (tailored) V-shape and a random planar composite (RPC) with the 50% coverage in the central plane of the system. These nanostructures are embedded in the dielectric host with the dielectric constant $\varepsilon_h=2.0$. We choose silver as the metal because it is a natural metal with the smallest dielectric losses in the visible and near infrared (ir) regions.[42] For silver as the metal component, the lifetime $\tau_n=1/(2\gamma_n)$, computed from Eq. (10), is shown in Fig. 2 as a function of the SP frequency.[47] This lifetime is maximum ≈ 60 fs in the near-ir region. For the coherent control to be effective, the pulse should be as long as possible, but not exceeding τ_n, qualitatively because the phase information is imprinted in the pulse as the change of the instantaneous periods in the excitation wave form. Therefore, the number of the phase degrees of freedom is $\sim T/\tau_n$, where T is the pulse duration. From these considerations, we choose $T=50$ fs and the carrier frequency of the pulse $\omega_0=0.8$ eV,

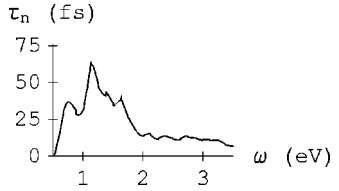

FIG. 2. Surface plasmon lifetime τ_n as a function of SP eigenfrequency ω.

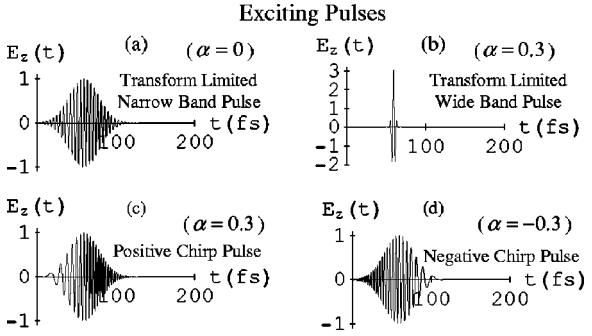

FIG. 3. Temporal dependence of the four excitation pulses studied with common parameters: $T=50$ fs, $\omega_0=0.8$ eV, and $E_0=1$. Panel (a), zero chirp ($\alpha=0$); panel (b), compressed (transform-limited) wide-band pulse ($\alpha=0.3$); panel (c), positive-chirp pulse ($\alpha=0.3$); panel (d) displays a negative-chirp pulse ($\alpha=-0.3$) (see text).

so a significant part of the near-ir region is within the pulse spectrum.

The eigenmodes and Green's function described in Sec. II depend only on the shape of the nanosystem, but not its size scale except for the trivial scaling of $\mathbf{r}$, $\mathbf{r}'$ with that size. However, the applicability of the present theory imposes conditions on the size scale. Those, apart from the condition of the quasistatic approximation $L \ll \lambda$, include also the limitations of the minimum size l. For the dielectric response to be local, l should be greater than the three characteristic intrinsic lengths of the system: electron mean-free path l_e, Debye screening radius r_D, and Fermi wavelength $\lambda\!\!\!^{-}_F$. Because in metals $l_e \gg r_D \gtrsim \lambda\!\!\!^{-}_F$, the condition $l \gtrsim l_e$ is violated first. For good metals such as silver or gold, $l_e \sim 5$–10 nm. In Fig. 1, the minimum size is two grid steps, which requires the grid step to be at least 3–5 nm; then the total size of the system is 60–100 nm, satisfying the quasistatic condition. When l becomes smaller, nonlocal effects may play important role. One of them is modeled as increase of the electron relaxation rate by a quantity $\gamma_{nl} \sim v_F/l$, where v_F is the electron velocity at the Fermi surface.[43] The closest systems studied experimentally that possess the maximum and minimum scale sizes on the same order as our systems were gold nanorods[44] (note that the V-shape is two nanorods connected at their end). This experiment not only does not show any increase of the resonance width corresponding to γ_{nl}, but, to the contrary, observes decrease of this width explained in Ref. 44 by the suppression of the interband transitions. In contrast to Ref. 43, the nonlocality affects mainly the spatial, not temporal, dispersion, as we argued in Ref. 45. These effects only become significant for l comparable with r_D, at distances on order of 1 nm or less.[45] Based on this, we will not consider the nonlocal effects in the present paper. Generally, to the best of our knowledge, among the wealth of publications on nano optics, the spatial dispersion has not so far been taken into account for any system more complex than a single nanosphere.

We consider four different exciting pulses shown in Figs. 3(a)–3(d). For the three of them [(a), (c), and (d)], the exciting field $\varphi_0(\mathbf{r},t)$ is a z-polarized chirped pulse with Gaussian envelope and duration T,

$$\varphi_0(\mathbf{r},t) = -z \exp\left\{ -i\omega_0\left(t-\frac{T}{2}\right)\left[1+\frac{2}{T}\alpha\left(t-\frac{T}{2}\right)\right] - \frac{3}{2T}\left[\left(t-\frac{T}{2}\right)\right]^2\right\} + \text{c.c.}, \tag{17}$$

where α is a dimensionless phase-modulation parameter. The fourth excitation pulse, panel (b), is a compressed one, computed for $|\alpha|=0.3$ as $\varphi_0(\mathbf{r},t)=\int e^{-i\omega t)}|\varphi_0(\mathbf{r},\omega)|\, d\omega/(2\pi)$, where $\varphi_0(\mathbf{r},\omega)$ is a Fourier transform of Eq. (17). Note that pulses (b)–(d) possess identical power spectra and differ only by frequency-phase modulation; pulses (a), (c), and (d) have identical temporal envelopes. Pulses (c) and (d) are time reversed (phase conjugated). All these pulses have the same average frequency. Comparison of the responses to them enables one to isolate effects of spectral composition and phase modulation. The integral intensity $Q^{(0)}$ for all these pulses is the same: it does not depend on the phase modulation or compression,

$$Q^{(0)} = \int [\mathbf{E}_0(t)]^2\, dt = \int |\mathbf{E}_0(\omega)]^2 \frac{d\omega}{2\pi}. \tag{18}$$

The characteristic function, $\Theta(\mathbf{r})$, that enters Eqs. (5) and (7) is a unit-step function whose gradient has a δ-function singularity. If Eqs. (5) and (7) are discretized directly, then this singularity may be lost, and the resulting solutions will be completely inaccurate. We took special care to deal with this edge singularity. We have chosen to smooth this singularity by applying a Gaussian filter, i.e., by replacing $\Theta(\mathbf{r}) \rightarrow \tilde{\Theta}(\mathbf{r})$, where

$$\tilde{\Theta}(\mathbf{r}) = \int \exp\left[\left(\frac{\mathbf{r}-\mathbf{r}'}{a}\right)^2\right]\Theta(\mathbf{r}')d^3r', \tag{19}$$

and a is the smoothing length. Computationally, we have carried out the integration in Eq. (19) using FFT method. We used $a=1$ grid step; our experience shows that increasing a does not change the solutions significantly. On the other hand, setting $a \rightarrow 0$, or using the original stepwise $\Theta(\mathbf{r})$ function would have brought about completely inaccurate results.

IV. COMPUTATIONAL RESULTS

A. V-shape: Transform limited excitation pulses

We display in Fig. 4 the kinetics of local fields for transform-limited excitation pulses at two characteristic points at the metal surface: the V shape opening (the widest part of the V shape) [panels (b) and (e)] and the apex of the V shape [(c) and (f)] along with the corresponding excitation pulses [(a) and (d)]. For the narrow-band pulse [panels (a)–(c)], the response at both the characteristic points has a smooth envelope where the pulse amplitude is significantly enhanced (by a factor of ≈ 25–50) with respect to the excitation pulse. The pulse at the apex is about twice higher than at the opening of the V shape, and both pulses are significantly extended in time (to ≈ 150 fs).

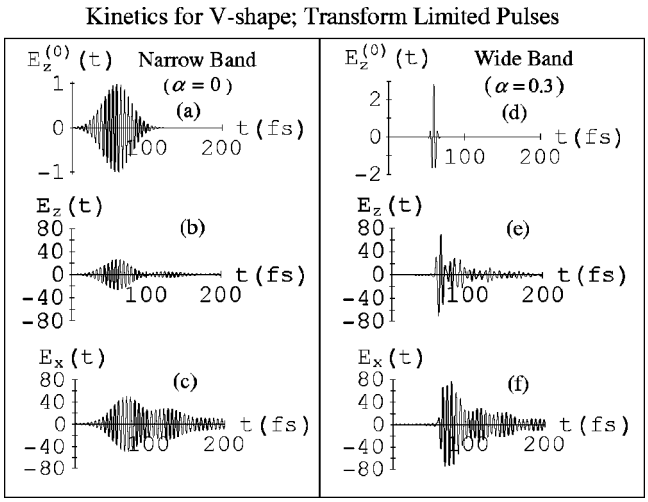

FIG. 4. Tranform-limited excitation pulses and the corresponding local fields for narrow-band excitation ($\alpha=0$) [panels (a)–(c)] and wide-band excitation ($|\alpha|=0.3$) [panels (d)–(f)]. Panels (b) and (e) display the local fields at the opening of the V shape, and panels (c) and (f) show the local fields at its apex. All pulses are shown in the same units and are directly comparable to each other. Silver used as a material for the V shape.

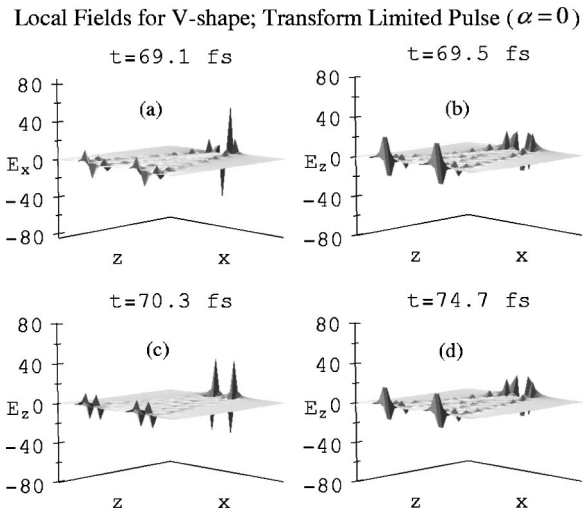

FIG. 5. For narrow-band unchirped pulse ($\alpha=0$), spatial dependence of the local fields in the plane of the V shape at its surface at the moments of time shown in the graphs. The spatial scale corresponds to Fig. 1, and the times correspond to Fig. 4. The magnitude of the fields is in the units of the excitation field E_0. For each moment, the maximum component x,y, or z of the local field that corresponds is displayed.

The wide-band pulse displayed in Figs. 4(d)–4(f) has the spectral width one order of magnitude greater than that for the narrow-band pulse. The excitation pulse is one full oscillation, and it is transform limited. Despite this extremely short duration of the excitation pulse, the local-field response of the V shape is as long as for the narrow-band pulse described above. At both the opening and apex of the V shape, the initial pulse of local fields is accompanied by a long period of ringing that is due to the existence of comparatively long living SP's within the spectral width of the excitation pulse.

More insight can be obtained from the spatial distribution of local fields. That for the case of the narrow-band transform-limited pulse is shown on Fig. 5. At the first moment shown [$t=69.1$ fs, panel (a)] corresponding approximately to the maximum of the exciting pulse, the fields are concentrated predominantly at the apex of the V shape where they enhanced by a factor of ≈ 45 with respect to the excitation field maximum magnitude E_0. However, in just 400 as, i.e., within the optical cycle, the maximum intensity is shifted to the opening [$t=69.5$ fs, (b)]. Then at less than 1 fs, this maximum returns to the apex [$t=70.3$ fs, (c)] and then continues to oscillate between the opening and the tip, never concentrating at one site [cf. panel (d)]. Thus continuing transfer of the excitation energy between the apex and the tip occurs in a fraction of the optical period during the entire duration of the pulse and beyond it (cf. Fig. 4). This is a reflection of the general effect of giant attosecond fluctuations:[17] continuous oscillations of the local-filed energy across the entire extent of a nanosystem during a fraction of the optical period.

The spatial distributions of local fields for the wide-band unchirped, ultrashort exciting pulse are shown in Fig. 6. Qualitatively, they behave similar to the narrow-band excitation shown in the previous figure: there are high local fields at the apex, and the energy is continuously transferred from apex to the opening and back, which is in agreement with the overlap in time of the local fields at the apex and opening of the V shape evident in Fig. 4, supporting the general concept of the giant attosecond fluctuations of local fields. Quantitatively, the maximum field is by a factor of ≈ 2 larger than in Fig. 5. Thus, the dramatic (more than one order of magnitude) broadening of the pulse spectrum and shortening of its duration, leads only to some quantitative, but not qualitative improvement in the localization of energy at the tip.

B. V-shape: Chirped excitation pulses

Kinetics of local fields at the opening and apex of the V shape is displayed in Fig. 7. Different from the transform-

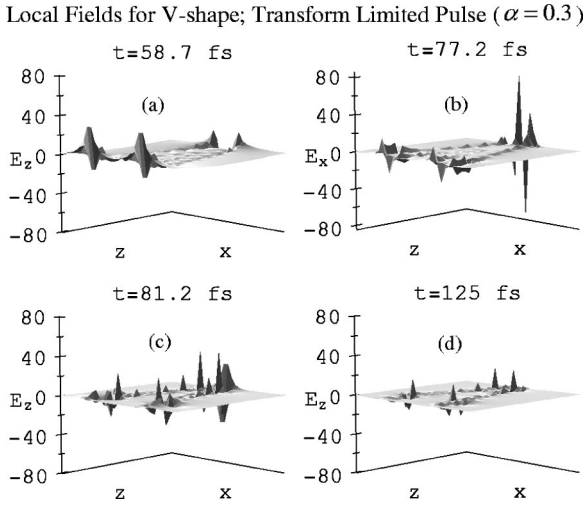

FIG. 6. Same as in Fig. 5, but for wide-band unchirped pulse ($|\alpha|=0.3$).

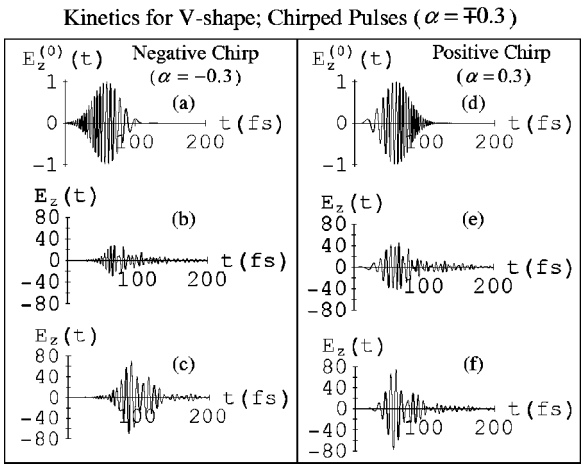

FIG. 7. Excitation pulses and the corresponding local fields for negatively chirped pulse ($\alpha = -0.3$) [panels (a)–(c)] and positively chirped pulse ($\alpha = 0.3$) [panels (d)–(f)]. Panels (b) and (e) display the local fields at the opening of the V shape, and panels (c) and (f) show the local fields at its apex. All pulses are shown in the same units and are directly comparable to each other. Silver used as a material for the V shape.

limited pulses (Fig. 4), the local-field pulse lengths are close to that of the exciting pulses: no significant ''ringing'' at long times is found. For the negative chirp, the local field at the opening [panel (b)] reaches its maximum simultaneously with the exciting field, while the field at the tip [panel (c)] is delayed with its maximum at $t \approx 100$ fs, i.e., practically after the end of the exciting pulse. In contrast, for the positively chirped pulse, the local fields [panels (e) and (f)] are concurrent in time with each other and with the exciting pulse. Thus, the negatively chirped pulse yields the selective concentration of the excitation energy at the tip of the nanostructure. Occurring after the end of the exciting pulse, this is clearly a coherent effect. For both the chirped excitation pulses, the field at the tip is greatly enhanced, by a factor of ≈ 80.

The spatial distributions for the case of the negatively chirped excitation are shown in Fig. 8 where we see that at the moment of time close to the maximum of the excitation pulse [$t = 57.3$, panel (a)], the local-field energy is concentrated at the opening of the nanostructure. However, at the end of the excitation pulse [$t = 80.3$–89.7 fs, panels (b) and (c)] the excitation energy is localized at the tip where it persists long after the excitation pulse has ended [$t = 118$ fs, panel (d)]. Thus, in this case, we achieve the desired concentration of the excitation energy at the tip of the V shape, where the local fields are enhanced by almost two orders of magnitude at their maxima with respect to the peak of the excitation pulse.

In contrast, for the positively chirped pulse, the spatial distributions of the local fields displayed in Fig. 9 show the energy concentration at the tip at the moment of time close to the excitation-pulse maximum [$t = 58.5$ fs, panel (a)]. The maximum of local fields moves to the opening of the V shape in less than two oscillation periods [$t = 64.3$ fs]. Then it moves back to the tip in approximately one oscillation period, still within the duration of the excitation pulse [$t = 68.3$ fs, panel (c)]. At comparatively long times [$t = 98.4$ fs, panel (d)], the local fields are essentially delocalized.

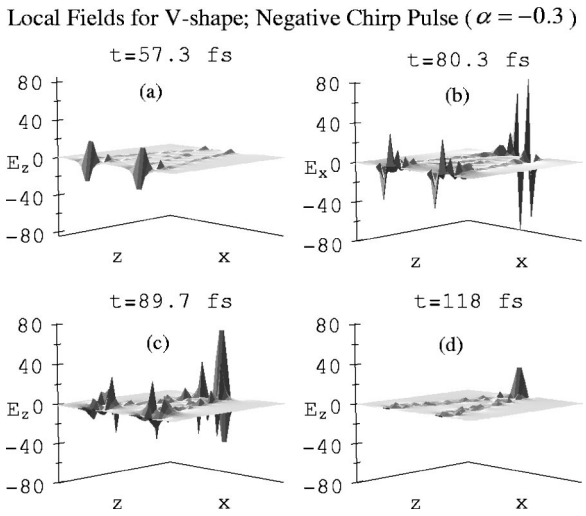

FIG. 8. For negatively chirped pulse ($\alpha = -0.3$), spatial dependence of the local fields in the plane of the V shape at its surface at the moments of time shown in the graphs. The spatial scale corresponds to Fig. 1, and the times correspond to Fig. 7. The magnitude of the fields is in the units of the excitation field E_0. For each moment, the maximum component x, y, or z of the local field that corresponds is displayed.

The significant difference in the spatiotemporal dynamic between the positively and negatively chirped pulses, which are time-reversed with respect to each other, necessarily shows that this dynamic is significantly not time reversible. This is certainly due to the dissipation in silver. This time-reversibility violation is significant despite very low dielectric losses in silver within the bandwidth of the excitation. We can interpret this fact as being due to the effect of chaoticity of dipolar eigenmodes:[26] this is similar to thermodynamic irreversibility of statistical physics despite the dynamic reversibility of the underlying exact quantum

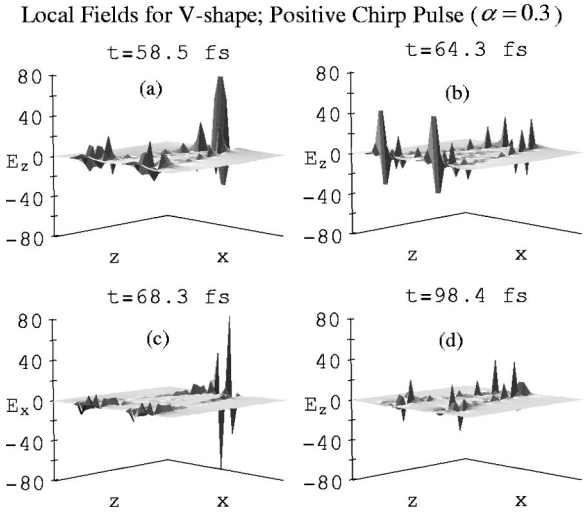

FIG. 9. Same as in Fig. 8, but for positively chirped pulse ($\alpha = 0.3$).

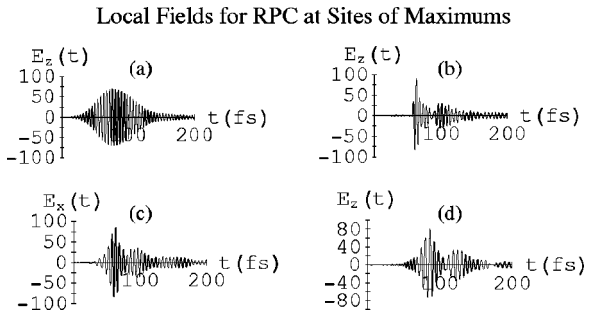

FIG. 10. For RPC, temporal dynamics of local fields for the four excitation pulses under consideration: narrow-band transform-limited (a), wide-band transform limited (b), negatively chirped (c), and positively chirped (d). In each case, the maximum component of the local field is shown at the spatial site of their corresponding global maximum.

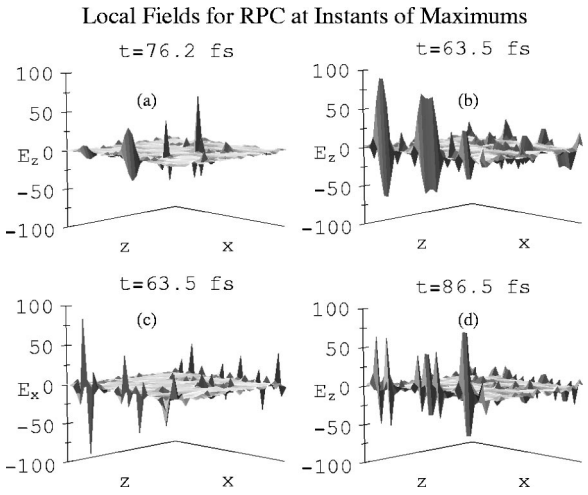

FIG. 11. Spatial distributions of local fields at the instances of their respective global maxima. The exciting pulses for panels (a) and (b) correspond to those in Fig. 10.

mechanics that is due to randomness and complexity of the eigenstates. Comparing the dynamics induced by the four excitation pulses presented above (Secs. IV A and IV B), we arrive at the conclusion that both the spectral composition and phase modulation of the excitation pulses significantly affect nanometer-femtosecond kinetics in metal nanostructures. With respect to the spectrum, it is somewhat obvious property, but the possibility to control this dynamics and concentrate the excitation local energy at a desired site of a nanosystem with the excitation-pulse phase modulation is nontrivial and potentially useful.

C. Random planar composites

For RPC, the kinetics of local fields induced by the four wave forms of the excitation pulses (at the spatial points where the global maximum is obtained in each case) is presented in Fig. 10. Panels (a)–(d) correspond to the excitation pulses of Fig. 3. Different from the V shape (cf. Fig. 7), there is a significant ''ringing'' of the induced local fields at times appreciably longer than the duration of the excitation pulse. Thus, in this case, it has been impossible to concentrate the local fields in time using the linear-chirped pulses. The amplitude of the response is higher for the wide-band pulses and reaches the value of ≈ 80, close to that for the V shape. In this case, the positive-chirped excitation [panel (d)] creates the maximum temporal delay of the response. This delay and ringing are the effects of the relatively long phase memory of silver in the spectral region considered.

The spatial distributions of the local fields for RPC at the moments when those fields reach their respective global maxima for the four excitation pulses under consideration are shown in Fig. 11. The field distribution for the case of the narrow-band pulses [panel (a)] shows a pronounced concentration of energy at a dominating peak where the enhancement $E_z \approx 60$. This concentration is unrelated to the phase modulation and is the manifestation of the ''ninth wave'' effect obtained earlier with the use of the dipole-dipole approximation.[16] A similar spontaneous concentration, but at two sites is also seen in panel (b) for the wide-band transform-limited pulse. In panel (c), the negatively chirped pulse excites a different distribution than that of panel (b). The positively chirped pulse [panel (d)] is significantly different from the above distributions, though it does not show any enhanced concentration of energy at a single location.

Thus for RPC, we could not show enhancement of the energy concentration using the linearly chirped pulse. Nevertheless, we have found that both the spectral composition and the phase modulation do affect the spatiotemporal dynamics. This still leaves open a possibility to control this dynamics by a more sophisticated phase modulation.

D. Mean linear fields and two-photon excitation

We introduce the time-averaged distribution of the local-field intensity

$$\langle I(\mathbf{r})\rangle = \frac{1}{T}\int_{-\infty}^{\infty} |\mathbf{E}(\mathbf{r},t)|^2 dt = \frac{1}{T}\int \frac{d\omega}{2\pi}|E_0(\omega)|^2 \left| 1 - \int z' \nabla'^2 G^r(\mathbf{r},\mathbf{r}',\omega) d^3 r' \right|^2, \tag{20}$$

which, obviously, depends only on the power spectrum, $|E_0(\omega)|^2$, but not on the phase of the excitation. Thus, *the average linear local-field intensities are not controllable by the phase modulation*. This conclusion is illustrated by the direct temporal integration of the numerically obtained solutions, whose results are shown in Fig. 12. Indeed, we see that the three pulses with identical spectra, namely, negatively chirped [panel (b)], positively chirped [panel (c)], and wide band [panel (d)], have the identical average intensity distribution $\langle I(\mathbf{r})\rangle$, which is an independent check that the computations are correct. In contrast, distribution $\langle I(\mathbf{r})\rangle$ for the transform limited narrow-band pulse [panel(a)] is completely different.

In sharp contrast to the average linear local intensity [cf. Eq. (20) and Fig. 12], there is no principle that forbids the coherent (i.e., by means of phase-modulation) control of the

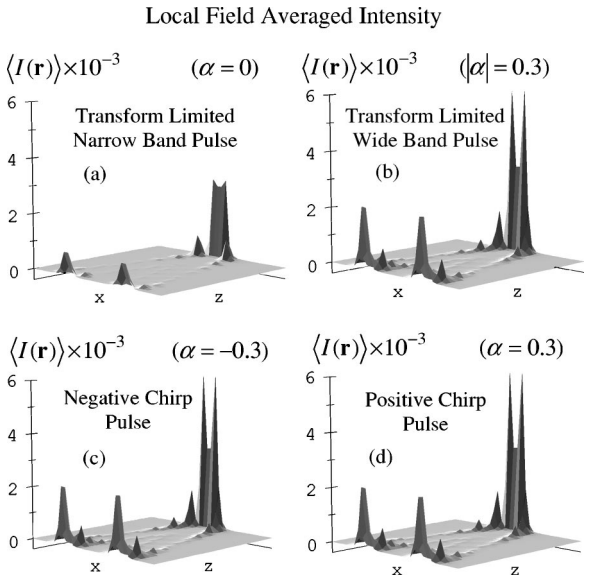

FIG. 12. Time-averaged spatial distributions $\langle I(\mathbf{r})\rangle$ of the local fields. Panels (a)–(d) correspond to those for the excitation pulses in Fig. 3.

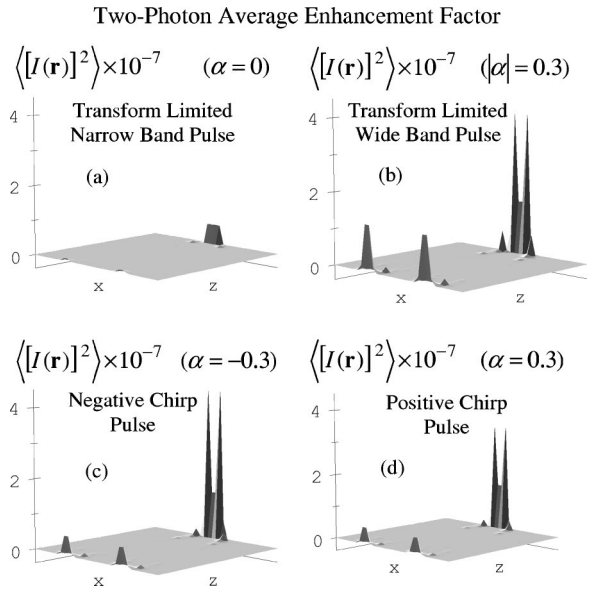

FIG. 13. Time-averaged spatial distributions of the local-field two-photon absorption enhancement $\langle[I(\mathbf{r})]^2\rangle$. Panels (a)–(d) correspond to those for the excitation pulses in Fig. 3.

average intensity of *nonlinear* processes. In Fig. 13, we show the average enhancement factor of the two-photon absorption calculated as

$$\langle[I(\mathbf{r})]^2\rangle = \int_{-\infty}^{\infty} |\mathbf{E}(\mathbf{r},t)|^4 dt. \tag{21}$$

From this we can clearly see that the negatively chirped pulse [panel (c)] produces the best concentration of the two-photon excitation at the tip of the V shape: it yields the highest intensity at the tip and the relatively small excitation at the opening. Note that this maximum enhancement is very significant, $\approx 4.5\times 10^7$, exceeding that for the narrow-band pulse by an order of magnitude. This supports the possibility to concentrate the integral nonlinear excitation at the desired site of a nanostructure. Importantly, the time-averaged local enhancement of SERS (surface-enhanced Raman scattering) is given approximately by same factor, $\langle[I(\mathbf{r})]^2\rangle$, as the two-photon excitation and is also very significant, $\approx 4.5\times 10^7$, and sharply localized at the tip of the V shape for the negative-chirp pulse.

V. CONCLUDING REMARKS

Without repeating the specific discussion presented in the preceding sections, here we very briefly summarize the major results. We have demonstrated a possibility to control the spatotemporal dynamics of a nanosystem on the nanometer-femtosecond scale. The degrees of freedom for such a control are provided by the spectral composition and spectral-phase modulation of the excitation pulse. The broadening of the spectrum of the excitation pulses to nearly one octave leads to a significant enhancement of the local fields at the tip of the V-shaped nanostructure. The spectral-phase modulation (at a constant spectral shape) of the excitation pulse allows one to concentrate the excitation at the tip of the V-shaped nanosystem at a certain time interval, in particular, achieve the duration of the local-field pulse close to that of the excitation pulse, without any long-time ''ringing'' tails. However, for the linear photoprocesses, the time-average local-field intensity are not phase controllable. In contrast, for nonlinear photoprocesses, the average yield can also be controlled by the phase modulation of the excitation pulse, which is demonstrated on the example of two-photon excitation.

The effects of coherently controlling the spatial concentration on the nanoscale and temporal course on the femtosecond scale of the ultrafast excitation energy in nanosystems may find applications in a wide range of optical probing and nanomodification of nanosystems. Some perspective areas of application comprise metal-nanostructure enhanced probing and spectroscopy, in particular, surface-enhanced Raman spectroscopy, of single molecules or chemical groups of larger molecules or biological objects. These applications include the temporal resolution due to the short duration of the local-field pulses. Nanomodification of the nanosystem, such as the local photochemical modification of large molecules, bio-objects, or surfaces may be another perspective area of applications.

ACKNOWLEDGMENTS

This work was supported by the Chemical Sciences, Biosciences, and Geosciences Division of the Office of Basic Energy Sciences, Office of Science, U.S. Department of Energy. Partial support for the work of D.J.B. was provided by grants from the US-Israel Binational Science Foundation and the Israel Science Foundation.

*Electronic address: mstockman@gsu.edu
URL: http://www.phy-astr.gsu.edu/stockman
†Electronic address: bergman@post.tau.ac.il
‡Electronic address: kobayashi@phys.s.u-tokyo.ac.jp

[1] H. Rabitz, R. de Vivie-Riedle, M. Motzkus, and K. Kompa, Science **288**, 824 (2000).
[2] R.J. Levis, G.M. Menkir, and H. Rabitz, Science **292**, 709 (2001).
[3] H. Rabitz, Science **299**, 525 (2003).
[4] M.M. Murnane, H.C. Kapteyn, S.P. Gordon, J. Bokor, E.N. Glytsis, and R.W. Falcone, Appl. Phys. Lett. **62**, 1068 (1993).
[5] T. Ditmire, T. Donnelly, R.W. Falcone, and M.D. Perry, Phys. Rev. Lett. **75**, 3122 (1995).
[6] L. Köller, M. Schumacher, J.T.J. Köhn, and K.H. Meiwes-Broer, Phys. Rev. Lett. **82**, 3783 (1999).
[7] S. Link, C. Burda, M. Mohamed, B. Nikoobacht, and M.A. El-Sayed, Phys. Rev. B **61**, 6086 (2000).
[8] B. Lamprecht, G. Schider, R.T. Lechner, H. Ditlbachter, J.R. Krenn, A. Leitner, and F.R. Aussenegg, Phys. Rev. Lett. **84**, 4721 (2000).
[9] T. Klar, M. Perner, S. Grosse, G. von Plessen, W. Spirkl, and J. Feldman, Phys. Rev. Lett. **80**, 4249 (1998).
[10] J. Lehmann, M. Mershdorf, W. Pfeifer, A. Thon, S. Voll, and C. Gerber, Phys. Rev. Lett. **85**, 2921 (2000).
[11] B. Lamprecht, J.R. Krenn, A. Leitner, and F.R. Aussenegg, Phys. Rev. Lett. **83**, 4421 (1999).
[12] J.-H. Klein-Wiele, P. Simon, and H.-G. Rubahn, Phys. Rev. Lett. **80**, 45 (1998).
[13] F. Stietz, J. Bosbach, T.W.T. Vartanyan, A. Goldmann, and F. Trägger, Phys. Rev. Lett. **84**, 5644 (2000).
[14] G. Kulcsár, D. AlMawlawi, F.W. Budnik, P.R. Herman, M. Moskovits, L. Zhao, and R.S. Marjoribanks, Phys. Rev. Lett. **84**, 5149 (2000).
[15] M. Perner, S. Gresillon, J. März, G. von Plessen, J. Feldmann, J. Porstendorfer, K.-J. Berg, and G. Berg, Phys. Rev. Lett. **85**, 792 (2000).
[16] M.I. Stockman, Phys. Rev. Lett. **84**, 1011 (2000).
[17] M.I. Stockman, Phys. Rev. B **62**, 10 494 (2000).
[18] M.I. Stockman, S.V. Faleev, and D.J. Bergman, Phys. Rev. Lett. **88**, 067402 (2002).
[19] D.J. Bergman and M.I. Stockman, Phys. Rev. Lett. **90**, 027402 (2003).
[20] T. Guenther, C. Lienau, T. Elsaesser, M. Glanemann, V.M. Axt, T. Kuhn, S. Eshlaghi, and A.D. Wieck, Phys. Rev. Lett. **89**, 057401 (2002); **89**, 179901(E) (2002).
[21] M.I. Stockman, Opt., Instrum. Data Proc. **3**, 27 (1989).
[22] K. Kneipp, Y. Wang, H. Kneipp, L.T. Perelman, I. Itzkan, R.R. Dasari, and M.S. Feld, Phys. Rev. Lett. **78**, 1667 (1997).
[23] S. Nie and S.R. Emory, Science **275**, 1102 (1997).
[24] A. Hartschuh, E.J. Sánchez, X.S. Xie, and L. Novotny, Phys. Rev. Lett. **90**, 095503 (2003).
[25] M.I. Stockman, L.N. Pandey, and T.F. George, Phys. Rev. B **53**, 2183 (1996).
[26] M.I. Stockman, Phys. Rev. Lett. **79**, 4562 (1997).
[27] M.I. Stockman, Phys. Rev. E **56**, 6494 (1997).
[28] M.I. Stockman, S.V. Faleev, and D.J. Bergman, Phys. Rev. Lett. **87**, 167401 (2001).
[29] R. Bartels, S. Bachus, E. Zeek, L. Misoguti, G. Vdovin, I.P. Christov, M.M. Murnane, and H.C. Kapteyn, Nature (London) **406**, 164 (2000).
[30] B.K. Dey, M. Shapiro, and P. Brumer, Phys. Rev. Lett. **85**, 3125 (2000).
[31] R.D.R. Bhat and J.E. Sipe, Phys. Rev. Lett. **85**, 5432 (2000).
[32] M.J. Stevens, A.L. Smirl, R.D.R. Bhat, A. Najmaie, J.E. Sipe, and H.M. van Driel, Phys. Rev. Lett. **90**, 136603 (2003).
[33] J. Hübner, W.W. Rühle, M. Klude, D. Hommel, R.D.R. Bhat, J.E. Sipe, and H.M. van Driel, Phys. Rev. Lett. **90**, 216601 (2003).
[34] Y.S. Kim, M. Tadi, H. Rabitz, A. Askar, and J.B. McManus, Phys. Rev. B **50**, 15 744 (1994).
[35] T. Feurer, J.C. Vaughan, and K.A. Nelson, Science **299**, 374 (2003).
[36] D.S. Citrin, Phys. Rev. Lett. **82**, 3172 (1999).
[37] R.A. Bartels, T.C. Weinacht, S.R. Leone, H.C. Kapteyn, and M.M. Murnane, Phys. Rev. Lett. **88**, 033001 (2002).
[38] D. J. Bergman and D. Stroud, in *Solid State Physics*, edited by H. Ehrenreich and D. Turnbull (Academic, Boston, 1992), Vol. 46, pp. 148–270.
[39] G. W. Milton, *The Theory of Composites* (Cambridge University Press, Cambridge, 2002).
[40] E. Anderson *et al.*, *LAPACK Users' Guide*, 2nd ed. (SIAM, Philadelphia, PA, 1995).
[41] *Intel Math Kernel Library Reference Manual*, Intel Corporation (1994-2002), Document Number 630813-6001.
[42] P.B. Johnson and R.W. Christy, Phys. Rev. B **6**, 4370 (1972).
[43] U. Kreibig and L. Genzel, Surf. Sci. **156**, 678 (1985).
[44] C. Sonnichsen, T. Franzl, T. Wilk, G. von Plessen, J. Feldmann, O. Wilson, and P. Mulvaney, Phys. Rev. Lett. **88**, 077402 (2002).
[45] I. A. Larkin, M. I. Stockman, M. Achermann, and V. I. Klimov, Phys. Rev. B (to be published).
[46] For the all-Dirichlet boundary conditions, there will be discontinuities of the field at the edges and vortices of the bounding prism. The periodic boundary conditions, on the other hand, cause spurious correlations between fields at the diametrally opposite sites of the system at its boundaries, which is undesirable.
[47] In Ref. 19, we have shown the time of the decay of electric fields, which is $1/\gamma_n$, i.e., twice greater than the present lifetime $\tau_n = 1/(2\gamma_n)$ that describes the decay of intensity.